Optics Letters

# MeV electron acceleration at 1 kHz with <10 mJ laser pulses

F. Salehi, A. J. Goers, G. A. Hine, L. Feder, D. Kuk, B. Miao, D. Woodbury, K. Y. Kim, and H. M. Milchberg*

*Institute for Research in Electronics and Applied Physics, University of Maryland, College Park, Maryland 20742, USA*
**Corresponding author: milch@umd.edu*

*Received 14 November 2016; revised 30 November 2016; accepted 30 November 2016; posted 1 December 2016 (Doc. ID 280796); published 6 January 2017*

**We demonstrate laser-driven acceleration of electrons to MeV-scale energies at 1 kHz repetition rate using <10 mJ pulses focused on near-critical density He and $H_2$ gas jets. Using the $H_2$ gas jet, electron acceleration to ~0.5 MeV in ~10 fC bunches was observed with laser pulse energy as low as 1.3 mJ. Increasing the pulse energy to 10 mJ, we measure ~1 pC charge bunches with >1 MeV energy for both He and $H_2$ gas jets.** 

***OCIS codes:*** (350.5400) Plasmas; (020.2649) Strong field laser physics; (320.2250) Femtosecond phenomena.

https://doi.org/10.1364/OL.42.000215

Laser-driven electron acceleration in plasma has become a well-established field since it was proposed several decades ago [1]. In recent years, significant experimental successes have been achieved, including the acceleration of quasi-monoenergetic electron bunches to ~4 GeV [2] and the generation of MeV-range gamma rays [3]. Typically, these experiments demand laser pulse energies of at least several joules and consequently existing laser technology limits them to low repetition rates (≤10 Hz).

There are numerous applications for MeV-scale electron beams where a compact and portable high-repetition-rate source is beneficial, especially for potential scanning purposes and improved data collection statistics. At low pulse repetition rates of ≤10 Hz, radiography using broadband, moderately divergent laser-plasma-accelerated electron beams from gas jets [4,5] or $\gamma$ rays from Bremsstrahlung conversion of the beam [6,7] has been demonstrated. Prior work at 0.5 kHz using a continuous-flow gas jet has produced ~100 keV, 10 fC electron bunches [8] and demonstrated their application to electron diffraction experiments [9]. While high-repetition-rate MeV acceleration of counter-propagating (~pC) electron bunches using solid and liquid targets has been reported [10,11], gas jet-based laser-plasma electron sources had yet to simultaneously achieve high-repetition-rate and forward-directed MeV-scale energies.

In nonplasma-based work, time-resolved electron diffraction using laser-driven photocathodes and conventional MeV accelerator structures such as LINACs is an established research area [12], where low emittance and narrow energy spreads are achieved. For <100 fs temporal resolution, this technique requires compensation for space charge effects and timing jitter [12].

The most common and successful laser-plasma-based acceleration scheme is laser wakefield acceleration (LWFA), which can be initiated by relativistic self-focusing of the laser pulse in the plasma. LWFA electron pulses can be ultrashort and are precisely timed to their driving optical pulses [13]. Relativistic self-focusing has a critical power [14] of $P_{cr} = 17.4\,(N_{cr}/N_e)$ GW, where $N_e$ is the plasma density, and $N_{cr}$ is the critical density. As $N_{cr} = 1.74 \times 10^{21}$ cm$^{-3}$ for the Ti:sapphire laser wavelength of $\lambda = 800$ nm, a very high $N_e$ is needed to keep $P_{cr}$ well below 1 TW and enable operation with current commercial laser technology for millijoule-scale pulses at 1 kHz. In previous experiments, we showed that using a high-density gas jet (at $N_e/N_{cr} < 0.25$) lowers $P_{cr}$ sufficiently to promote relativistic self-focusing and self-modulated laser wakefield acceleration (SM-LWFA) with subterawatt laser pulses [15]. In this Letter, we show that using gas jets approaching even closer to critical density ($N_e/N_{cr} < 0.69$) makes possible electron acceleration to relativistic energies with pulse energies as low as 1.3 mJ, delivered at 1 kHz. We note that for pulse propagation near $N_e/N_{cr} = 0.25$, the stimulated Raman scattering associated with SM-LWF generation can compete with the two-plasmon decay instability [16]. To help understand the details of acceleration in this regime, we present particle-in-cell (PIC) simulations later in this Letter.

Driving laser-plasma accelerators at high repetition rate using a gas jet target demands a nearly continuous flow out of a high-pressure nozzle. This leads to high background chamber pressure, which can enhance the deleterious effects of laser-induced ionization and defocusing well before the pulse encounters the gas jet. Our experiments demonstrate electron acceleration at chamber background pressures as high as 20 Torr, enabling use of continuous-flow nozzles and even higher repetition rate laser systems for LWFA. Figure 1 shows the experimental setup along with a measured He gas density profile, an accelerated electron beam profile, corresponding electron energy spectra, and interferograms and simulation results showing laser-generated plasma in the He and $H_2$ jets.

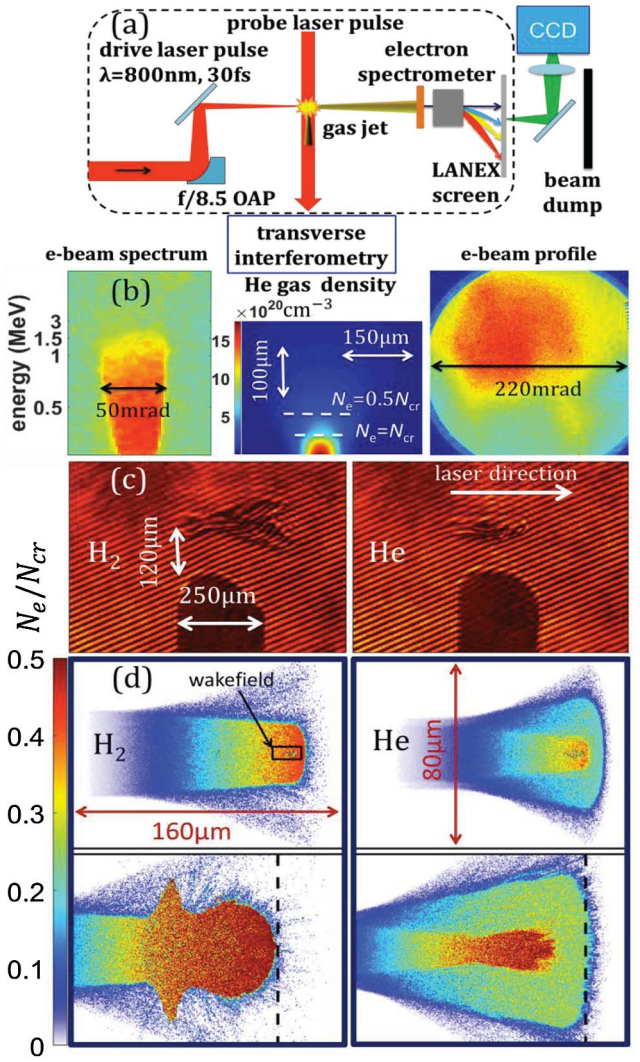


**Fig. 1.** (a) Experimental setup for high-repetition-rate electron acceleration. The dashed line depicts the vacuum chamber boundary. (b) Measured density profile for the He gas jet (center), electron beam profile from 20 consecutive shots at 1 kHz with 9.5 mJ pulse energy on the He jet (right), and corresponding electron energy spectrum (left). The sharp left–right edges on the spectrum are from electron beam clipping on the spectrometer magnet. (c) Interferograms showing residual plasma ~1 ps after interaction of 5 mJ pulses with $H_2$ and He gas jets. The dark shadow is the gas nozzle. (d) Electron density profiles before (top) and 250 fs after wave breaking (bottom) from 2D PIC simulations of the interaction of 5 mJ, 30 fs laser pulses with 200 μm FWHM $H_2$ and He jets at a peak neutral density of $4.35 \times 10^{20}$ molecules or atoms per $cm^3$. The dashed vertical lines indicate the center of the gas jet.

We used $\lambda = 800$ nm, 30 fs, <12 mJ pulses from a 1 kHz Ti:sapphire laser to drive LWFA in the dense jets. The pulses were tightly focused with an $f/8.5$ off-axis paraboloid to a 9 μm intensity FWHM spot size. Given the risk of a high accumulated gamma radiation dose from running the experiment at 1 kHz, we used a solenoid valve before the nozzle to control the gas flow duration.

Gas jet density and plasma profiles were measured using folded wavefront interferometry [17] with a $\lambda = 800$ nm probe split from the main pulse. High-density $H_2$ and He gas jets were produced by cooling the gas to −150°C at 1100 psi and flowing the gas through a 150 μm nozzle into a vacuum chamber pumped by a 220 CFM roots blower. The gas jet density encountered by the laser pulse was controlled by changing the backing pressure, temperature, and the location of the laser focus on the jet. As determined from interferometry, the jet density has a Gaussian transverse profile of FWHM 150–250 μm depending on the laser focus position. Within ~60 μm of the nozzle exit, we achieve $N_e/N_{cr} \sim 1$ at full ionization. To reduce nozzle damage, the laser was focused at least 110 μm above the nozzle orifice, where $N_e/N_{cr} \sim 0.5$. Accelerated electron spectra were collected 35 cm beyond the jet by a magnetic spectrometer consisting of a compact permanent 0.08 T magnet located behind a 1.7 mm wide copper slit, followed by a LANEX scintillating screen imaged onto a low-noise CCD camera. Day-to-day experimental runs for similar jet opening times gave slightly varying electron bunch energies and charges owing to gas jet nozzle tip erosion from plasma ablation. Nozzles were replaced after approximately $2 \times 10^5$ laser shots.

Figure 2 shows accelerated electron spectra from the $H_2$ jet for several values of laser pulse energy and with 10 ms valve open time. The inset shows the total charge per shot accelerated to >1 MeV energy versus laser pulse energy. Each point is the average of 10 consecutive shots. The exponential electron spectra and the moderately collimated beams of Fig. 1 are evidence of SM-LWFA, reflecting acceleration from strongly curved plasma wave buckets and wave-breaking electron injection into a range of accelerating phases [15]. Lowering the laser pulse energy requires increasing the electron density to maintain $P > P_{cr}$. The minimum electron density required to observe electron acceleration with 9 mJ pulses was $4.0 \times 10^{20}$ $cm^{-3}$ ($N_e/N_{cr} = 0.23$). To observe acceleration for 1.3 mJ pulses, it was necessary to increase the electron density to $1.2 \times 10^{21}$ $cm^{-3}$ ($N_e/N_{cr} = 0.69$).

At low laser pulse energies (<3 mJ) with $H_2$ jets, most of the electrons are at energies below our spectrometer range. Moving the spectrometer out of the electron beam path allows the full beam to impact the LANEX (shielded by 25 μm

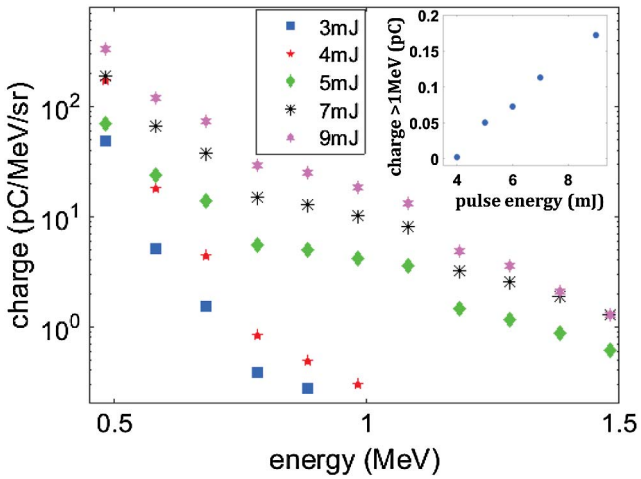


**Fig. 2.** Accelerated electron energy spectra from $H_2$ jets for varying laser pulse energies and 10 ms gas jet open time. The inset shows the total charge with >1 MeV energy versus laser pulse energy. The ±0.05 MeV energy bins correspond to the magnetic spectrometer's coarsest energy resolution (at 1.5 MeV).

aluminum foil). Using the electron transmission data for aluminum [18] and the LANEX response [19,20], we estimate electron bunches of ~10 fC charge with up to ~0.5 MeV energy for laser pulse energies as low as 1.3 mJ.

Using He jets, no electron beams were detected for laser pulses <5 mJ. For both $H_2$ and He jets, increasing the pulse energy to ~10 mJ increased the bunch charge with >1 MeV energy to ~1 pC. We attribute these observations to ionization-induced defocusing in He at low laser pulse energy. The transverse electron density profile in the $H_2$ jet is flatter than in the He jet owing to a lower threshold for full ionization in $H_2$ [21], resulting in less defocusing in $H_2$ and larger amplitude plasma waves. This is borne out by interferograms [Fig. 1(c)] showing the residual plasma ~1 ps after interaction of a 5 mJ pulse with the He and $H_2$ jets. The associated 2D PIC simulations [Fig. 1(d)] using the code TurboWave [22] show the electron density profiles just before and 250 fs after plasma wave breaking in the $H_2$ and He jets—it is seen that the hydrogen plasma profile is fully ionized over a wider region than in He and that the post-wave-breaking scatter of the laser pulse and electron heating in hydrogen gives a wider profile at the jet exit.

Figure 3(a) shows accelerated electron spectra for varying peak electron density from the He jet using 9.5 mJ pulses and a 20 ms valve open time. Corresponding total charge accelerated to >1 MeV is shown in the inset. Figure 3(b) shows electron beam profiles on LANEX for selected He plasma densities of Fig. 3(a), showing the sensitivity to plasma density. While the total accelerated charge increases significantly with peak electron density, the normalized electron spectrum does not change noticeably. The beam divergence angle (estimated from an average around the 50% beam intensity contour) is ~150 mrad at $N_e/N_{cr} = 0.25$ and increases to ~260 mrad as the electron density is increased to $N_e/N_{cr} = 0.43$.

A major concern using a high-density continuous-flow gas jet is the background pressure buildup inside the target chamber, which can lead to ionization-induced defocusing of the pulse. In order to study the effect of background pressure buildup, we first measured accelerated electron spectra for increasing valve open times (with the laser at 1 kHz and the jet repetition rate at 0.5 Hz), as shown in Fig. 4, where a He gas jet at $N_e/N_{cr} = 0.54$ is driven by 10 mJ laser pulses. It is seen that increasing the valve open time lowers the charge per shot while keeping the normalized spectra similar. The charge per shot at >1 MeV decreases from ~1.6 to ~0.2 pC as the opening time increases from 1 to 100 ms, over which the corresponding background pressure increases from <0.1 to ~3.5 Torr.

Increasing the valve open time to 1 s, with a repetition rate of 0.5 Hz, increases the background pressure to a constant ~20 Torr. Scanning a 50 ms window (containing a 50 shot burst of 10 mJ pulses) over the 1 s valve opening of the He jet gives a nearly unchanging LANEX signal. This shows that the valve could be open continuously if the accumulation of the gamma ray dose from our beam stop was not a constraint.

To better understand SM-LWF generation and acceleration in our jet at electron densities above quarter critical ($N_e/N_{cr} > 0.25$), we performed 2D PIC simulations for 4 mJ laser pulses interacting with a 200 μm FWHM preionized $H_2$ target with a peak of $N_e/N_{cr} = 0.5$. Figure 5 shows the simulated plasma wake just before and after wave breaking (top) and the corresponding central lineouts (bottom) of electron density and normalized laser vector potential $a_0$. The

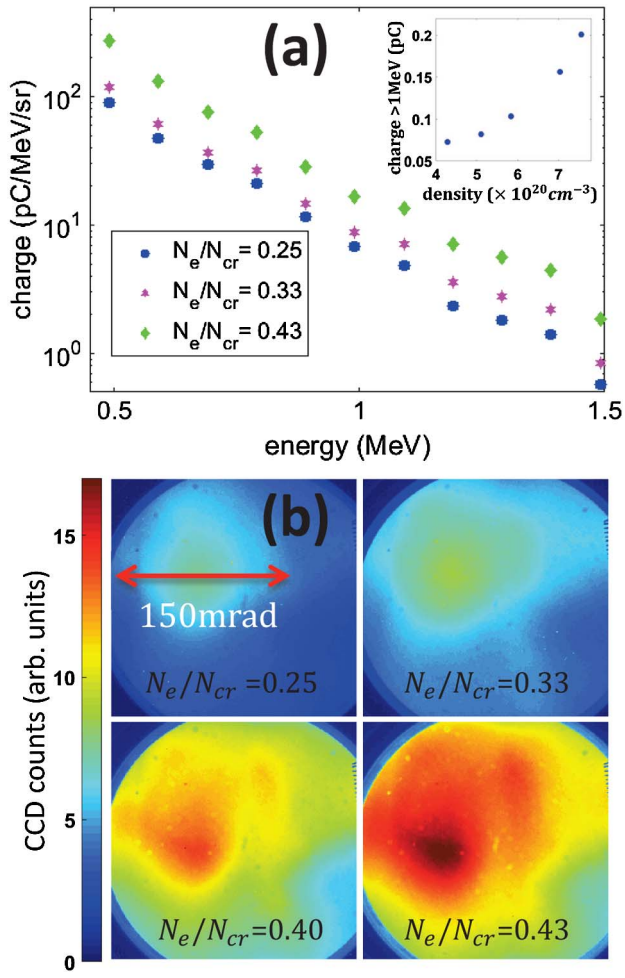


**Fig. 3.** (a) Electron energy spectrum for varying plasma densities from the He jet using 9.5 mJ laser pulses and a 20 ms gas jet open time. The inset shows the total charge per shot with >1 MeV energy. (b) Electron beam profiles on the LANEX screen, illustrating sensitivity to plasma density. The outside circle is the outline of the vacuum port, through which the LANEX surface was imaged.

wakefield is generated at an ambient plasma density above quarter critical (dashed line), where the Raman Stokes line is suppressed and the anti-Stokes line dominates, as seen in the forward-directed optical spectrum shown. Two-plasmon decay is not evident over the full laser propagation, possibly due to the strongly nonlinearly steepened density in the plasma wake [23].

For our prior experiments at high density, PIC simulations showed that both LWFA and direct laser acceleration (DLA) contributed to electron energy gain, with LWFA dominating at lower laser pulse energies [15]. For the current experiments with ≤10 mJ pulses, PIC simulations show that LWFA dominates DLA up to the highest plasma densities used. The simulations also show that the leading part of the electron bunch is 30–60 fs FWHM for our range of laser and plasma conditions, followed by a longer (>100 fs) low-energy tail. The simulated spectrum, shown in Fig. 4, indicates approximately 10× more charge than measured, along with a higher effective temperature than in the experimental spectra, differences we are currently trying to resolve.

In summary, we have demonstrated for the first time, to our knowledge, laser-driven electron acceleration to >1 MeV in a

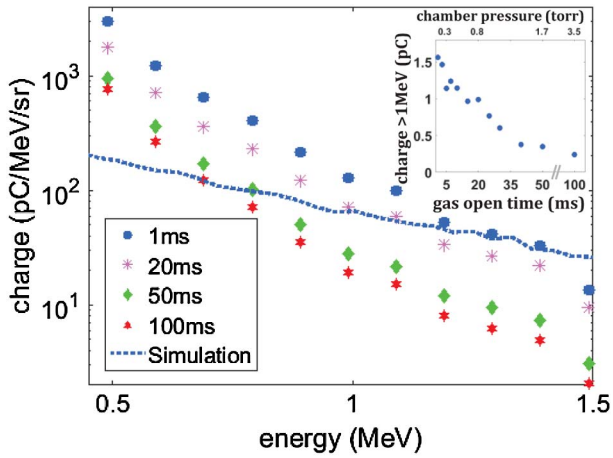


**Fig. 4.** Electron energy spectrum per shot from the He gas jet ($N_e/N_{cr} = 0.54$) for different valve open times for 10 mJ laser pulses at 1 kHz. Inset: total charge per shot accelerated to >1 MeV and corresponding background pressure. The dashed blue line shows the spectrum (×0.1) from a 3D PIC simulation of one shot for $N_e/N_{cr} = 0.5$ and 10 mJ.

gas jet using a 1 kHz repetition rate mJ-scale laser, with bunch charge to the pC level. This result was made possible by use of a thin, dense, gas jet target enabling near-critical density laser interaction. Our source can be useful for time-resolved probing of matter for scientific, medical, or security applications, either using the electrons directly or using a high-Z foil converter to generate ultrafast $\gamma$ rays.

**Funding.** U.S. Department of Energy (DOE) (DESC0010706TDD, DESC0015516); Air Force Office of Scientific Research (AFOSR) (FA95501310044); National Science Foundation (NSF) (PHY1535519); U.S. Department of Homeland Security (DHS) (2016DN077ARI104).

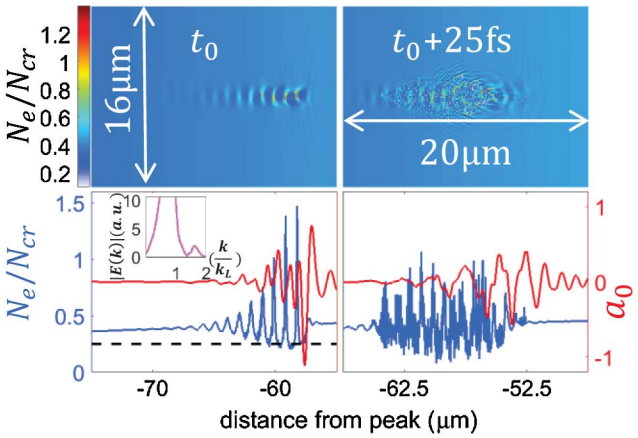


**Fig. 5.** Simulated plasma wake just before and after wave breaking (top) and corresponding central lineouts (bottom) of density and normalized laser vector potential for a 4 mJ pulse interacting with a 200 μm FWHM preionized $H_2$ target of peak $N_e/N_{cr} = 0.5$. Dashed line: $N_e/N_{cr} = 0.25$. Inset: the pre-wave-breaking spectrum of the self-modulated laser showing the anti-Stokes line, with the Stokes line suppressed.

**Acknowledgment.** The authors thank Yungjun Yoo for help with the laser. Simulations were performed using University of Maryland supercomputing resources (http://www.it.umd.edu/hpcc).

## REFERENCES

1. T. Tajima and J. M. Dawson, Phys. Rev. Lett. **43**, 267 (1979).
2. W. P. Leemans, A. J. Gonsalves, H. S. Mao, K. Nakamura, C. Benedetti, C. B. Schroeder, C. S. Toth, J. Daniels, D. E. Mittelberger, S. S. Bulanov, J. L. Vay, C. G. R. Geddes, and E. Esarey, Phys. Rev. Lett. **113**, 245002 (2014).
3. S. Cipiccia, M. R. Islam, B. Ersfeld, R. P. Shanks, E. Brunetti, G. Vieux, X. Yang, R. C. Issac, S. M. Wiggins, G. H. Welsh, M. P. Anania, D. Maneuski, R. Montgomery, G. Smith, M. Hoek, D. J. Hamilton, N. R. C. Lemos, D. Symes, P. P. Rajeev, V. O. Shea, J. M. Dias, and D. A. Jaroszynski, Nat. Phys. **7**, 867 (2011).
4. S. P. D. Mangles, B. R. Walton, Z. Najmudin, A. E. Dangor, K. Krushelnick, V. Malka, M. Manclossi, N. Lopes, C. Carias, G. Mendes, and F. Dorchies, Laser Part. Beams **24**, 185 (2006).
5. C. G. Bussolino, A. Faenov, A. Giulietti, D. Giulietti, P. Koester, L. Labate, T. Levato, T. Pikuz, and A. L. Gizzi, J. Phys. D. **46**, 245501 (2013).
6. A. Döpp, E. Guillaume, C. Thaury, A. Lifschitz, F. Sylla, J. Goddet, A. Tafzi, G. Iaquanello, T. Lefrou, P. Rousseau, E. Conejero, C. Ruiz, K. T. Phuoc, and V. Malka, Nucl. Instrum. Methods Phys. Res. A **830**, 515 (2016).
7. R. D. Edwards, M. A. Sinclair, T. J. Goldsack, K. Krushelnick, F. N. Beg, E. L. Clark, A. E. Dangor, Z. Najmudin, M. Tatarakis, B. Walton, M. Zepf, K. W. D. Ledingham, I. Spencer, P. A. Norreys, R. J. Clarke, R. Kodama, Y. Toyama, and M. Tampo, Appl. Phys. Lett. **80**, 2129 (2002).
8. Z. H. He, B. Hou, J. A. Nees, J. H. Easter, J. Faure, K. Krushelnick, and A. G. R. Thomas, New J. Phys. **15**, 053016 (2013).
9. Z. H. He, A. G. R. Thomas, B. Beaurepaire, J. A. Nees, B. Hou, V. Malka, K. Krushelnick, and J. Faure, Appl. Phys. Lett. **102**, 064104 (2013).
10. A. G. Mordovanakis, J. Easter, N. Naumova, K. Popov, P. E. Masson-Laborde, B. Hou, I. Sokolov, G. Mourou, I. V. Glazyrin, W. Rozmus, V. Bychenkov, J. Nees, and K. Krushelnick, Phys. Rev. Lett. **103**, 235001 (2009).
11. S. Feister, D. R. Austin, J. T. Morrison, K. D. Frische, C. Orban, G. Ngirmang, A. Handler, M. Schillaci, E. A. Chowdhury, R. R. Freeman, and W. M. Roquemore, "Super-ponderomotive electron spectra from efficient, high-intensity, kHz laser-water interactions," arXiv:1508.07374 (2015).
12. R. J. D. Miller, Science **343**, 1108 (2014).
13. E. Esarey, C. B. Schroeder, and W. P. Leemans, Rev. Mod. Phys. **81**, 1229 (2009).
14. G. Z. Sun, E. Ott, Y. C. Lee, and P. Guzdar, Phys. Fluids **30**, 526 (1987).
15. A. J. Goers, G. A. Hine, L. Feder, B. Miao, F. Salehi, J. K. Wahlstrand, and H. M. Milchberg, Phys. Rev. Lett. **115**, 194802 (2015).
16. C. Z. Xiao, Z. J. Liu, C. Y. Zheng, and X. T. He, Phys. Plasmas **23**, 022704 (2016).
17. T. R. Clark and H. M. Milchberg, Phys. Rev. Lett. **78**, 2373 (1997).
18. National Institute of Standards and Technology, http://physics.nist.gov/PhysRefData/Star/Text/ESTAR.html.
19. Y. Glinec, J. Faure, A. Guemnie-Tafo, V. Malka, H. Monard, J. P. Larbre, V. De Waele, J. L. Marignier, and M. Mostafavi, Rev. Sci. Instrum. **77**, 103301 (2006).
20. A. Buck, K. Zeil, A. Popp, K. Schmid, A. Jochmann, S. D. Kraft, B. Hidding, T. Kudyakov, C. M. S. Sears, L. Veisz, S. Karsch, J. Pawelke, R. Sauerbrey, T. Cowan, F. Krausz, and U. Schramm, Rev. Sci. Instrum. **81**, 033301 (2010).
21. S. Augst, D. D. Meyerhofer, D. Strickland, and S. L. Chin, J. Opt. Soc. Am. B **8**, 858 (1991).
22. D. F. Gordon, IEEE Trans. Plasma Sci. **35**, 1486 (2007).
23. A. B. Langdon, B. F. Lasinski, and W. L. Kruer, Phys. Rev. Lett. **43**, 133 (1979).